ARMY RESEARCH LABORATORY

Techniques for the Health Assessment of Automotive Alternators

by Andrew J. Bayba, David N. Siegel, and Kwok Tom

ARL-TR-6041   **June 2012**

NOTICES

Disclaimers

The findings in this report are not to be construed as an official Department of the Army position unless so designated by other authorized documents.

Citation of manufacturer's or trade names does not constitute an official endorsement or approval of the use thereof.

Destroy this report when it is no longer needed. Do not return it to the originator.

Army Research Laboratory

Adelphi, MD 20783-1197

ARL-TR-6041   **June 2012**

Techniques for the Health Assessment of Automotive Alternators

Andrew J. Bayba, David N. Siegel, and Kwok Tom
Sensors and Electron Devices Directorate, ARL

REPORT DOCUMENTATION PAGE

Form Approved
OMB No. 0704-0188

1. REPORT DATE *(DD-MM-YYYY)* June 2012	2. REPORT TYPE Final	3. DATES COVERED (From - To) August to October 2011	
4. TITLE AND SUBTITLE Techniques for the Health Assessment of Automotive Alternators		5a. CONTRACT NUMBER	
		5b. GRANT NUMBER	
		5c. PROGRAM ELEMENT NUMBER	
6. AUTHOR(S) Andrew J. Bayba, David N. Siegel, and Kwok Tom		5d. PROJECT NUMBER 2NE6KK	
		5e. TASK NUMBER	
		5f. WORK UNIT NUMBER	
7. PERFORMING ORGANIZATION NAME(S) AND ADDRESS(ES) U.S. Army Research Laboratory ATTN: RDRL-SER-E 2800 Powder Mill Road Adelphi, MD 20783-1197		8. PERFORMING ORGANIZATION REPORT NUMBER ARL-TR-6041	
9. SPONSORING/MONITORING AGENCY NAME(S) AND ADDRESS(ES)		10. SPONSOR/MONITOR'S ACRONYM(S)	
		11. SPONSOR/MONITOR'S REPORT NUMBER(S)	
12. DISTRIBUTION/AVAILABILITY STATEMENT Approved for public release; distribution unlimited.			
13. SUPPLEMENTARY NOTES			

14. ABSTRACT

Preliminary data analysis was performed on automotive alternators in common use in Army vehicles. This effort was an investigation on the feasibility of early fault detection using data analysis techniques. Using data acquired on a common military vehicle alternator, several analysis methods were employed to arrive at features expected to indicate anomalous behavior. This specific data analysis task supports the broader objective to investigate the feasibility of real-time condition monitoring and failure mode diagnostics in Army systems.

15. SUBJECT TERMS

Alternator health assessment, alternator health monitoring, alternator prognostics and diagnostics

16. SECURITY CLASSIFICATION OF:			17. LIMITATION OF ABSTRACT	18. NUMBER OF PAGES	19a. NAME OF RESPONSIBLE PERSON Andrew J. Bayba
a. REPORT Unclassified	b. ABSTRACT Unclassified	c. THIS PAGE Unclassified	UU	46	19b. TELEPHONE NUMBER *(Include area code)* (301) 394-0440

Standard Form 298 (Rev. 8/98)
Prescribed by ANSI Std. Z39.18

Contents

List of Figures

List of Tables

INTENTIONALLY LEFT BLANK.

1. Introduction

Automated prognostics and diagnostics (P&D) of the health of Army assets has become a top Department of Defense (DoD) priority. This is particularly true in the automotive field due to the sheer quantity of vehicles in service. The alternator has been identified as an item where P&D could have a significant impact. Alternator testing was performed by the Applied Research Laboratory at Pennsylvania State University (PSU) under contract from the U.S. Army Tank and Automotive Research, Development and Engineering Command (TARDEC). The testing performed by PSU was to characterize various alternators with the intention of conducting seeded fault testing. A limited number of alternators were characterized due to redirection of the PSU effort to another project. Six alternators were tested: three new and three used. The alternators are Leece-Neville 4000 Series, model number A0014827 JB 130A. Additional information can be found in the PSU Report of the testing (*1*). The used alternators had no obvious indication of damage. Curiously, one of the new alternators had a catastrophic failure during the course of testing. This failed alternator provided us the opportunity to search for precursor indicators of failure, in addition to developing characteristic baseline features for discriminating between new and used alternators.

This study provides valuable information on the relevance of various analysis techniques for the assessment of alternator health and significant observations regarding key features in the processed data. However, development of algorithms for P&D of alternator health would require additional data. By its nature, the PSU test data set does not lend itself to thorough diagnostic analysis, such as health assessment, and prognostics such as remaining useful life. This data set was only a baseline characterization of a subset of alternators available; the project was redirected prior to its completion and controlled fault testing never initiated. For proper diagnostic and prognostic algorithm development the alternators would require multiple runs at an operating set point, and runs for longer durations (some until failure). The PSU data set is lacking in both of these categories. However, we believe that our analysis of the data at hand is still very useful as various analysis techniques are examined and recommendations are presented for future work.

As a general note on performance of the alternators, all closely matched the expected relationship with output current and rotational speed according to the manufacturer's data sheet (*2*), as shown in figure 1. Alternator #5 measurements are prior to its failure.
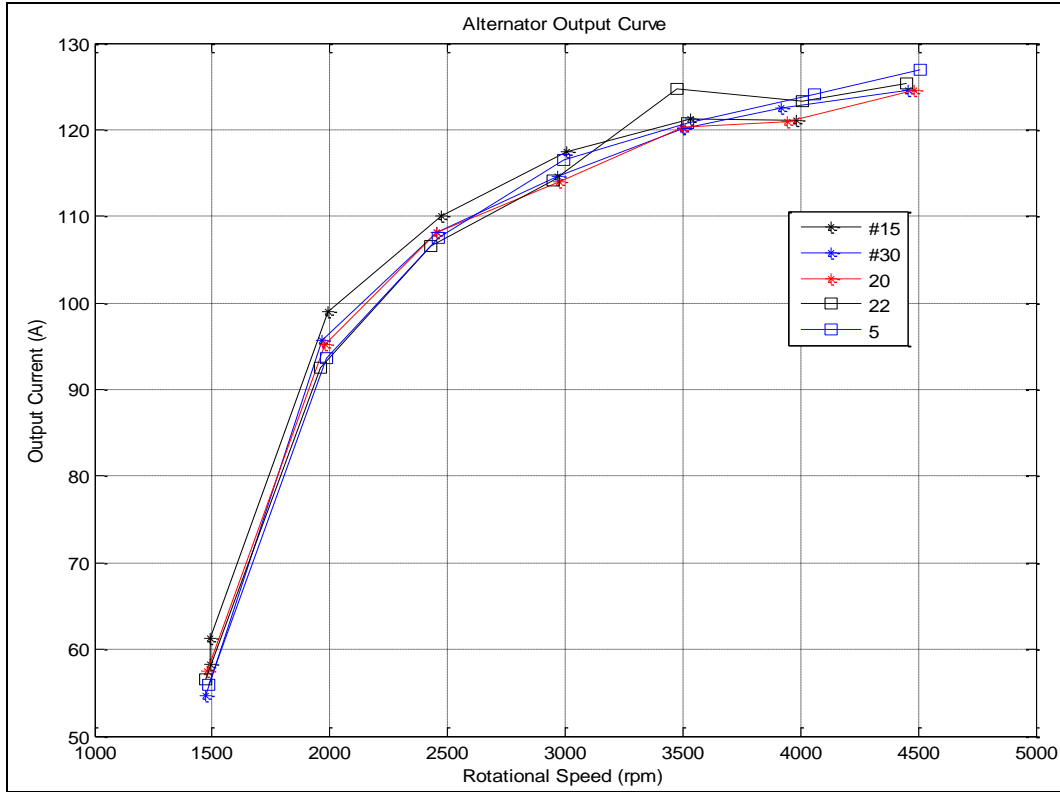
Figure 1. Output current of alternators as a function of rotational speed.

2. PSU Experiment Description

PSU performed two different series of experiments, hereafter referred to as Method 1 and Method 2. In Method 1, the current, rotational speed and ambient temperature were varied. In Method 2, the alternators were run at a given rotational speed at their maximum output current. Six alternators were tested in Method 1; the same alternators were testing in Method 2, except for #13. The reason for the exclusion of alternator #13 from Method 2 testing is unknown. Identification numbers were assigned to the alternators by PSU, and for clarity, the same designations have been retained here. Alternator numbers, condition, and comments are provided in table 1.

Table 1. Numbering and descriptions of alternators tested.

Alternator Identifier	Starting Condition	Comments
# 5	New	**Failed** during Run # 67 Method 2 test; output current and voltage dropped to near zero
# 13	New	Was not tested during the second set of tests (Method 2)
# 15	New	—
# 20	Used	—
# 22	Used	—
# 30	Used	—

1. In Method 1, the current, rotational speed and ambient temperature were varied; operating at specific set-points for each of the alternators, as shown in table 2. From table 2, one can calculate that each alternator was tested under 75 different operating points (5 current set-points, 5 speed set-points, and 3 temperature set-points). This produced 75 data files collected for each alternator. Since there were 6 alternators tested, a total of 450 data files were generated.

Table 2. Method 1 operating set-points

Current Setting (Amps)	Rotational Speed (RPM)	Ambient Temperature (°C)
10	1500	50
40	3000	100
70	4500	150
100	6000	
130	7500	

2. In the second set of experiments, Method 2, the alternators were operated at a given rotational speed in order to obtain the maximum output current for a given speed, as shown in table 3. This was essentially running the alternator at its output current set-points. Again, the same alternators were tested with the Method 2 procedure with the exception of alternator #13. During testing with Method 2, alternator #5 failed at some point in the second day of operation.

Table 3. Method 2 operating points.

Current Output (Amps)	Rotational Speed (RPM)
60	1500
95	2500
107	3000
115	3500
120	4000
125	4500

3. Data

Output current, output voltage, and the signals from the three axes of a tri-axial accelerometer comprised the measured data, as shown in table 4. The data were sampled at 102.4 KHz for all five channels. There is no tachometer signal; however, alternative methods were used to synthesize a tach signal so that certain analysis techniques could be employed. Measurement of the individual phase voltages and currents was not acquired, but would be very useful if future studies are conducted.

Table 4. Data collected.

Signal	Signal Description	Comments
1	Vibration - x	From tri-axis accelerometer
2	Vibration – y	From tri-axis accelerometer
3	Vibration – z	From tri-axis accelerometer
4	Output Current	From current transducer on the 28-V terminal
5	Output Voltage	Voltage signal from 28-V terminal

4. Signal Processing Techniques

The approach taken was to evaluate various signal processing techniques as to their applicability of identifying anomalies associated with degradation, health assessment, and prediction.

We first consider recent automotive alternator condition monitoring work to get an idea of what the primary faults are and what approaches are being used (table 5). It appears that the common alternator failure modes are diode faults, stator winding faults, belt slippage, and bearing faults. The two patents that employ the root-mean-square (RMS) ratio between phase currents should be noted. Their implementation appears to have significant potential due to the ease and low cost of insertion and the relative simplicity of processing. Unfortunately, we could not pursue this area since individual phase currents were not recorded.

Table 5. Recent work in alternator health monitoring.

Company/University/ Research Center	Methods	Comments
Caterpillar (3)	RMS ratio between each of the three phase currents	This patent precedes the C. E. Niehoff patent
C. E. Niehoff (4)	RMS ratio between phase currents also includes control aspects for handling the degraded situation.	They are an Original Equipment Manufacturer of alternators, so they could potentially embed the intelligence into the component.
General Motors R&D, also includes Wright State University (5–7)	Data driven Principal Component Analysis and various residual model based algorithms	Focused on belt slippage and diode problems.
AMSSA and Applied Research Lab at Penn. State University (8)	Current and vibration time and frequency domain analysis, and feature extraction techniques	Seeded fault test with stator winding short and bearing faults showed promise
Clemson University (9)	Model-based residual method, automatically set thresholds using their approach	For detecting belt slippage, diode, and regular problems, the paper shows simulation results

There are many signal processing techniques that can be employed on the alternator data set in order to generate features that might be useful for condition monitoring. Extracting features or condition indicators from the vibration, voltage, and current sensor measurements provides deeper comprehension of the alternator operational condition. Basic statistical conversion of the measured sensor data provides a means of reducing and summarizing the sensor output to a few parameters. Some of the other techniques enhance the signal quality through noise reduction or filtering. Analysis is also conducted in the frequency domain, where certain physical characteristics of the alternator can be easily recognized. These along with the rationale are presented in table 6.

Table 6. Signal processing techniques employed in this report.

Technique	Rationale
Time Domain Analysis	Voltage waveform has various signatures related to stator or diode faults (*10, 11*).
Frequency Domain Analysis	Harmonics (36X/stator slot frequency); sub harmonics (12X or 18X), and sidebands could be important (*12*).
Time Synchronous Averaging	Improve signal to noise ratio for harmonics synchronous with shaft (18X, 36X, 72X, etc.) (*13*).
Analysis of the Residual Signal	Analogous to gear signals, stator slot frequency vibration and current information (36X) can be removed and residual signal can offer diagnostic information.
Envelope Demodulation	Demodulation around 36X can reveal sidebands and amplitude modulation effects.
Bearing High Frequency Response Technique (HFRT)-Envelope Analysis	Most established method for bearing condition monitoring (*14*).

4.1 Time Domain Waveform Analysis

Time domain waveform analysis is the easiest to perform and is potentially sufficient for diagnostics and prognostics. Statistical features such as RMS, peak to peak, and kurtosis are easy to calculate, making them amenable to real-time application, and in many cases, are good indicators of degradation. Samples of the raw signal data are presented below since several characteristics of interest are clearly visible.

4.1.1 Time Domain Current Signals

Figures 2 and 3 show sample plots of current time signals for two new alternators; figure 3 is immediately prior to failure of alternator #5. As seen in the figures, the signals distinctly show a clear ripple frequency of 36 times the alternator shaft speed (36X). The plots are shown for a single period with the alternator rotating at a nominal rate of 3500 rpm and an electrical load in the range of 120–130 A. This ripple frequency is based on their being six pole pairs, three phases, and the rectification of each phase by the diodes producing 36 "ripples" for each rotation (3 x 6 x 2). Even though figure 3 is right before the failure of alternator #5, there is very little visual difference in the time domain between the signals of the two figures.
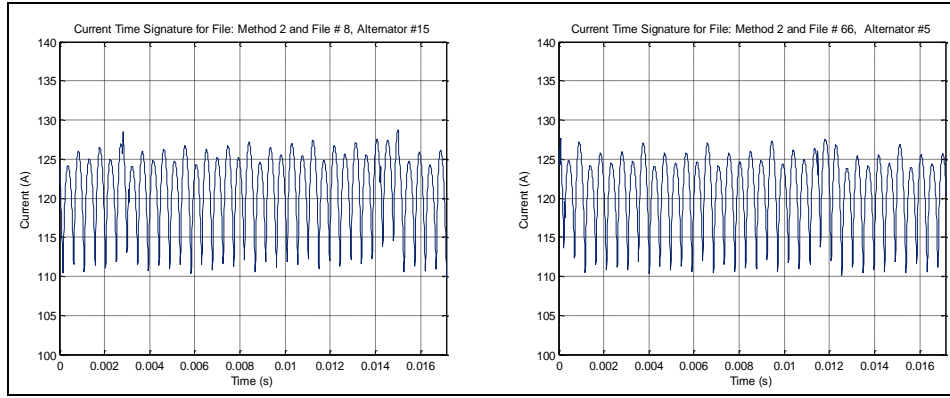
Figure 2. (a) Current signal of a new alternator and (b) alternator #5 just prior to failure.
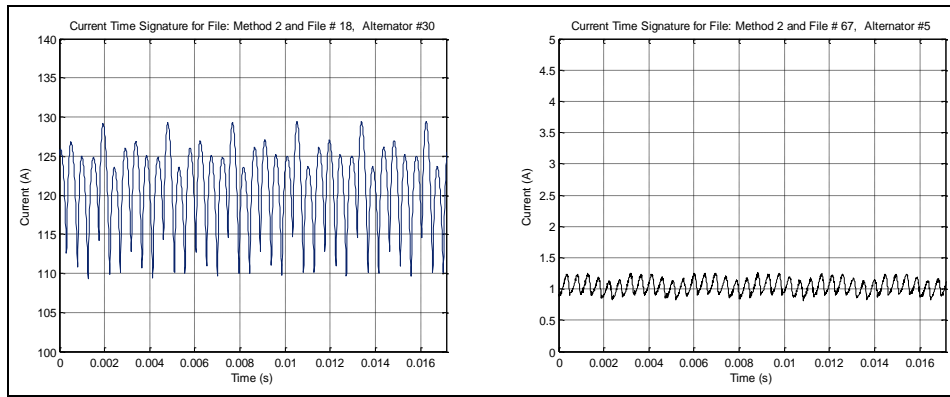

Figure 3. (a) Current signal of a used alternator and (b) alternator #5 immediately after failure.

The current signal for a used alternator is shown in figure 3a and from alternator #5 immediately after failure in figure 3b. The used alternator shows the 36X ripple frequency along with amplitude modulation, in which the modulation frequency is approximately 6X. One can observe in figure 3b that the output of the alternator that failed is only at 1A output current. It still retains a frequency of 36X.

4.1.2 Time Domain Voltage Signals

The voltage signal also shows a characteristic ripple frequency for new alternators (#13 and #5 just prior to failure), as is seen in figures 4a and b. Visually, there is not a substantial difference in the two time signals.
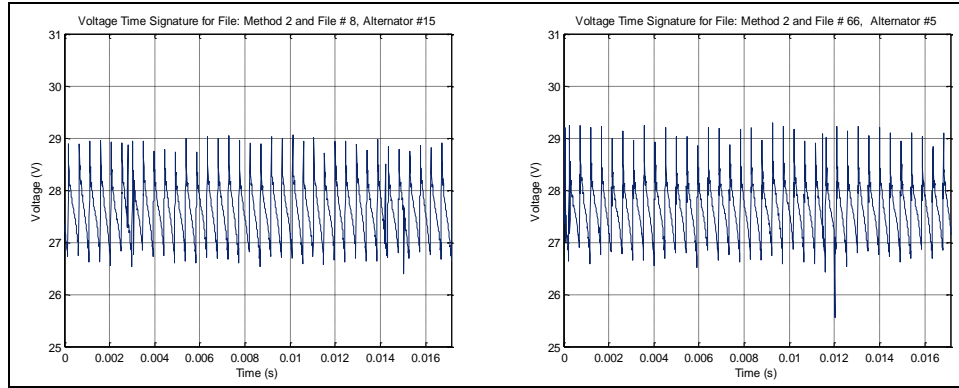
Figure 4. (a) Voltage signal of a new alternator and (b) alternator #5 just prior to failure.

The used alternator shows a visually similar voltage time signal (figure 5a) compared to a new alternator. Figure 5b is the voltage signal of the failed alternator and as seen, the failure signature is very obvious; not only is the voltage output much lower, a clear 6× frequency can be observed.
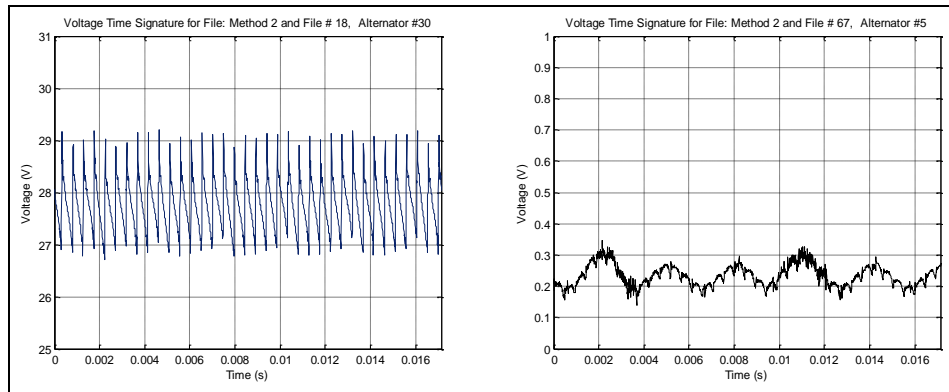

Figure 5. (a) Voltage signal of a used alternator and (b) alternator #5 immediately after failure.

4.2   Frequency Domain Processing and Key Harmonics

In this category, there are specific frequencies (key harmonics) to monitor and additional frequency domain information that can be examined. The key harmonics to be monitored are listed in table 7, where X is a multiple (order) of the shaft frequency. Other spectral components are related to the physical configuration of the alternator and briefly explained. Each individual phase voltage and current signal prior to rectification has a fundamental frequency of 6 times the shaft speed. Also, shaft vibration at 1X the shaft speed due to unbalance or 2X due to misalignment could also be present, as well as harmonics. Finally, there are several frequencies of interest related to bearing tones, which are discussed in more detail in section 4.8.

8

Table 7. Key harmonics to monitor.

Signal	Frequency (Orders)	Comments
Current	36X* and harmonics	Ripple frequency, due to 6 poles, 3 phases, and rectification.
Voltage	36X* and harmonics	Ripple frequency, due to 6 poles, 3 phases, and rectification.
Vibration	36X* and harmonics	Stator slot frequency, 36 stator slots and each pass generates a magnetic force.

4.3 Current and Voltage Spectra

The current and voltage spectra are presented for new, used, and pre- and post-failure alternators in figures A-1 and A-2 of the appendix. The current and voltage spectra have a very similar structure for all cases and the following observations apply to both. The frequency spectra show clear peaks at the ripple frequency, 36X, and its harmonics (up to 180X) for all the cases. An example plot of a new alternator is presented in figure 6, displaying the 36X peak and harmonics. A visual inspection of the current and voltage spectra (in the appendix) revealed some interesting observations. The spectra are very much similar for all the operational alternators. A 36X component is easily observed. Even the failed alternator has peaks at 36X and its harmonics; however, the magnitudes are much, much lower than the other cases. The used alternator has a peak at 12X, which is not observed for any of the new alternators.
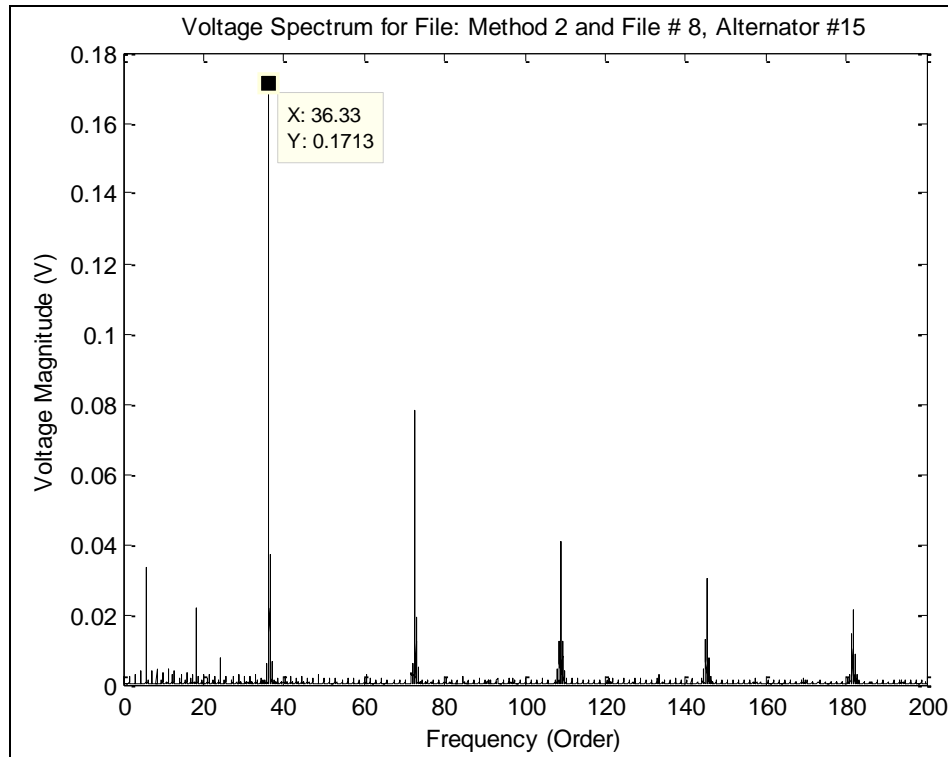
Figure 6. Typical voltage spectrum for a functional alternator.

9

4.4 Vibration Spectra

X, Y, and Z-direction accelerometer spectra are presented for a new, used, and pre- and post-failure alternator (#5) in figures A-3, A-4, and A-5 of the appendix. In comparing the spectra of a new alternator, the pre-failure alternator and a used alternator spectra, one can see a clear peak at the stator slot frequency (36X) in all cases and that the 36X peaks are reasonably close in magnitude. The difference in magnitude of these sample plots was later seen to be within the variation of all the alternators (pre-failure). The failed alternator has no frequency content at 36X or harmonics of 36X. One curious result in the Y-direction is that for both the pre- and post-failure alternators, there is a significant peak at 3X; this may be due to shaft-related problems such as misalignment or imbalance. The Z-direction accelerometer spectrum contains isolated high frequency content as broadband responses between orders 50 and 60 (near 3000 Hz) and also between orders 100 and 120 (near 6000 Hz). The failed alternator also contains the high frequency content indicating that this phenomenon is related to structural resonances and not due to the magnetic forces from the rotor passing each stator slot. Example plots of interest are included here for reference. Figure 7 shows the distinct 36X peak present in all pre-failure alternators, figure 8 shows the 3X peak in alternator #5 in the Y-direction, and figure 9 shows the high frequency broadband responses in the Z-direction.
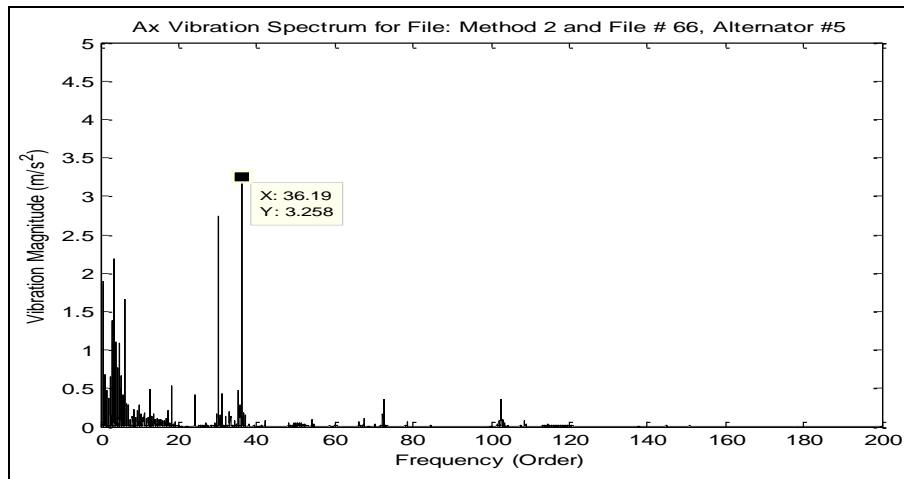

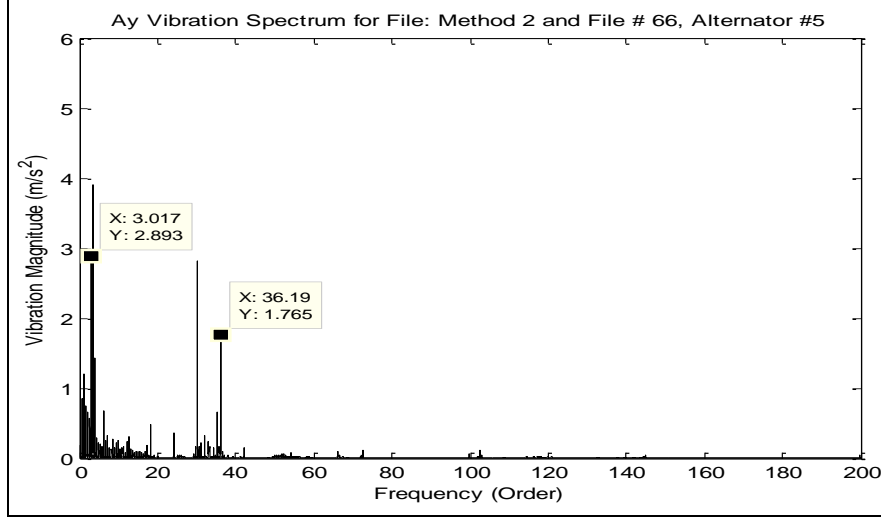Figure 7. Functional alternator spectrum showing the typical 36X peak.

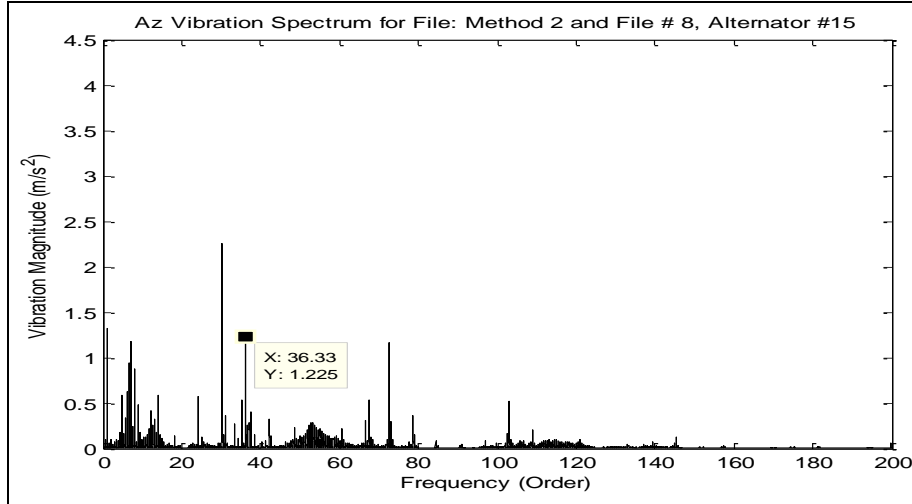Figure 8. Y-direction spectrum of alternator #5 showing the 3X peak.

Figure 9. Z-direction of alternator #5 showing high frequency content.

4.5   Time Synchronous Averaging

As the name implies, time synchronous averaging (TSA) averages multiple blocks of data and is done in order to improve the signal-to-noise ratio. In order to employ this method, blocks of data must be synchronized. This is commonly done by synchronizing the start of each data block with a tachometer (tach) pulse. However, in this experiment a tach pulse was not recorded. Since the nominal speed of the shaft is known, we can use the data itself to derive a precise speed because of the presence of the 36X frequency component. With a precise speed, we can synthesize a tach pulse, which will serve as our synchronization mechanism. The steps for the aforementioned operation were previously described for gear meshing (*15*) and are detailed as follows:

11

1. Bandpass filter the input signal around the 36X peak.

2. Take the Hilbert Transform of the filtered signal.

3. Calculate the phase of the analytic signal and unwrap the phase.

4. Take the modulus of the unwrapped phase signal over 2P.

With this synchronization technique, it is now possible to apply the standard TSA methodology. In this technique, we find the zero crossings of the tach signal, interpolating the signal of interest at N equally spaced samples for each shaft revolution and ensemble averaging the re-sampled signal. Example spectra of the synchronous averages are provided in the appendix (figures A-6 through A-10) and show that most of the spectral lines are distinct order harmonics. Also, the 36X peak has a noticeably higher magnitude ratio to other spectral lines compared to the non-averaged signal.

4.6 Residual and Regular Signal Processing

These methods employ the concept that the synchronous signal can be divided into components, which can be further analyzed. As shown in equation 1, the signal can be divided into $x_{regular}(t)$, whose content is always present irrespective of the alternator condition or operating point and includes 36X and harmonics; $x_{residual}(t)$, which possesses only the sidebands and sub-harmonics of the ripple frequency; and $x_{shaft}(t)$, which is the content related to shaft vibration unrelated to sidebands or sub-harmonics. Since these components contain particular information of the signal, it allows for the extraction of unique and potentially useful features associated with that component. The component $x_{shaft}(t)$ is expected to be unrelated to the alternator degradation and is not considered further in this study. Figures A-11 and A-12 in the appendix show residual signals for the current and voltage, respectively, for the four alternator cases.

$$x_{synchronous}(t) = x_{regular}(t) + x_{residual}(t) + x_{shaft}(t)$$

(1)

4.7 Envelope Analysis

The concept is to refine the examination of amplitude modulation affects around the ripple frequency/stator slot frequency. The processing steps include filtering around the 36X peak and using the Hilbert Transform to extract the envelope signal. Statistics of the envelope signal can then be processed in addition to examining the spectra. The rationale for including this method is that information related to sidebands, as well as amplitude modulation, can be captured. Sample plots for the current and voltage envelope signals are presented in the appendix (figures A-13 and A-14, respectively).

4.8 Bearing Fault Analysis

Bearing defects/damage is always an important consideration when analyzing rotating machinery. Bearing health is assessed by analysis involving the bearing characteristic

frequencies, commonly referred to as fault frequencies. The bearing fault frequencies were calculated using the standard equations given in equations 2–5: The resulting orders/frequencies are listed in table 8. It is important to note that the frequencies presented assume no slipping, while in reality, the actual values will vary slightly.

$$BPFI = \frac{n}{2}\left(1 + \frac{BD}{PD}\cos\theta\right) * f \qquad (2)$$

$$BPFO = \frac{n}{2}\left(1 - \frac{BD}{PD}\cos\theta\right) * f \qquad (3)$$

$$FTF = \frac{1}{2}\left(1 - \frac{BD}{PD}\cos\theta\right) * f \qquad (4)$$

$$BSF = \frac{PD}{2BD}\left(1 - (BD/PD)^2\cos^2\theta\right) * f \qquad (5)$$

where

BPFI = the ball pass frequency of the outer race

BPFO = the ball pass frequency of the outer race and corresponds to a defect on the outer race

FTF = the fundamental train frequency

BSF = the ball spin frequency

f = the shaft frequency

n = number of balls

BD = ball diameter

PD = pitch diameter

θ = contact angle

Table 8. Fault frequencies as a function of shaft frequency (order) and the special case of 3500 RPM.

Bearing Fault Frequency	Order	Frequency at 3500 RPM (Order * Shaft Frequency)
BPFO	2.61	152.05 Hz
BPFI	4.39	256.28 Hz
BSF	1.83	106.82 Hz
FTF	0.37	21.72 Hz

Usually for incipient bearing damage, it is difficult to see bearing fault frequency peaks in the traditional spectrum (*14*). A very effective method to look for the fault frequencies is to perform envelope analysis; this method is well established for bearing condition monitoring. The procedure here is the same as that used previously for envelope analysis; however, the frequency

13

that is bandpassed around is the natural or resonance frequency instead of the ripple frequency. The bearing incipient fault is easier to detect at the resonance frequency band due to the amplification in this band over the noise corruption resident in the low frequency band. A bandpass filter centered around 3000 Hz was used, since there was a distinct natural frequency excited in this frequency range. The magnitudes of the fault frequencies are then recorded as features, as well as statistical information. Example plots of envelope vibration spectra are provide in figure A-15 in the appendix.

4.9   Figures of Merit

Certain features were calculated from combinations of other features based on their potential to provide better indicators of degradation; these metrics were termed figures of merit (FOMs). These same set of FOMs are calculated for both the voltage and current signal. The vibration signal includes the first three, but replaces the last one with a ratio between the HFRT envelope RMS and the RMS of the raw signal.

The first, FOM_0, is given in equation 6, and provides the percentage of the signal comprised of 36X and harmonics compared distinct with the total signal content synchronous with the shaft (values of 0.9 or above were typical):

$$FOM\_0 = \left(\frac{RMS_{RegularSignal}}{RMS_{TSASignal}} \right)^2 \tag{6}$$

The second, FOM_1, given in equation 7 provides a percentage of the signal is left if one removes the frequency content to due to ripple signal and harmonics (36X):

$$FOM\_1 = \left(\frac{RMS_{ResidualSignal}}{RMS_{TSASignal}} \right)^2 \tag{7}$$

The third, FOM_2, given in equation 8 is the ratio between the 18X peak and 36X peak. Prior work by PSU suggested this metric (8).

$$FOM\_2 = \left(\frac{18X\_Peak}{36X\_Peak} \right) \tag{8}$$

Finally, FOM_3, given in equation 9 provides a normalization of the ripple magnitude by the 36X peak; both are known to increase with RPM and electrical load.

$$FOM\_3 = \left(\frac{Ripple\_Magnitude}{36X\_Peak} \right) \tag{9}$$

4.10 Feature Extraction and Selection

In an effort to capture any changes in the signal, features were extracted for analysis. As can be seen in table 9, statistical features that are commonly used as indicators of degradation were extracted for time domain signals, specific frequency peaks were extracted from the frequency domain, and there are a few special features such as the FOMs.

Table 9. Features extracted.

#	Signal	Processing Method	Features	#Features
1	Raw Signal	Time Domain	RMS, peak to peak, kurtosis	15 (3 for each signal)
2	Time Synchronous Signal	Time Domain	RMS, peak to peak, kurtosis	15 (3 for each signal)
3	Regular Signal	Time Domain	RMS, peak to peak, kurtosis	15 (3 for each signal)
4	Residual Signal	Time Domain	RMS, peak to peak, kurtosis	15 (3 for each signal)
5	Envelope Signal	Time Domain	RMS, peak to peak, kurtosis	15 (3 for each signal)
6	Vibration HFRT Envelope Signal	Time Domain	RMS, peak to peak, kurtosis	9 (3 for each vibration channel)
7	Ripple Feature Calculation	-	Mean, STDEV	4 (2 for current and voltage signal)
8	Envelope Signal	Frequency Domain	Peaks at 1X and 6X	10 (2 for each signal)
9	Time Synchronous Signal	Frequency Domain	1X-3X, 6X,12X…108X	105 (21 for each signal)
10	Raw Signal	Frequency Domain	BPFO, BPFI, BSF, FTF, and harmonics	24 (8 for each vibration signal)
11	HFRT Envelope Signal	Frequency Domain	BPFO, BPFI, BSF, FTF, and harmonics	24 (8 for each vibration signal)
12	Figure of Merit Features	-	-	20 (4 for each signal)

From the large array of extracted features, it is common practice to use algorithms to downselect features that show correlation or trending as a function of degradation, which may then be use to determine the state of health of the system. However, this feature set is not amenable to this type

of the analysis. The primary reason is that there are many data files but only a few at each operating point. This makes it difficult to use common feature selection ranking methods such as the fisher criterion, since the number of data samples in each class for a given operating point is small (*16*). In addition, the feature selection method is usually tuned for a specific aspect, such as classification. Considering these points, a visual screening of the features was done in order to examine which, if any, of the features were of interest. Figures 10–17 show plots of features that were deemed promising for future work. Discussion is incorporated with the figures. Note that figure 10 is from Method 1 testing and that figures 11 through 17 are from Method 2. Also, that in figures 11–17 that the plotting order on each graph starts with the new alternator #15, then the three used alternators #30, #20, and #22, and finally the new alternator that failed (#5)

As shown in figure 10, all the used alternators have a much higher 12X voltage peak than the new alternators. In the used alternators, a clear linear relationship with alternator speed can also be seen.
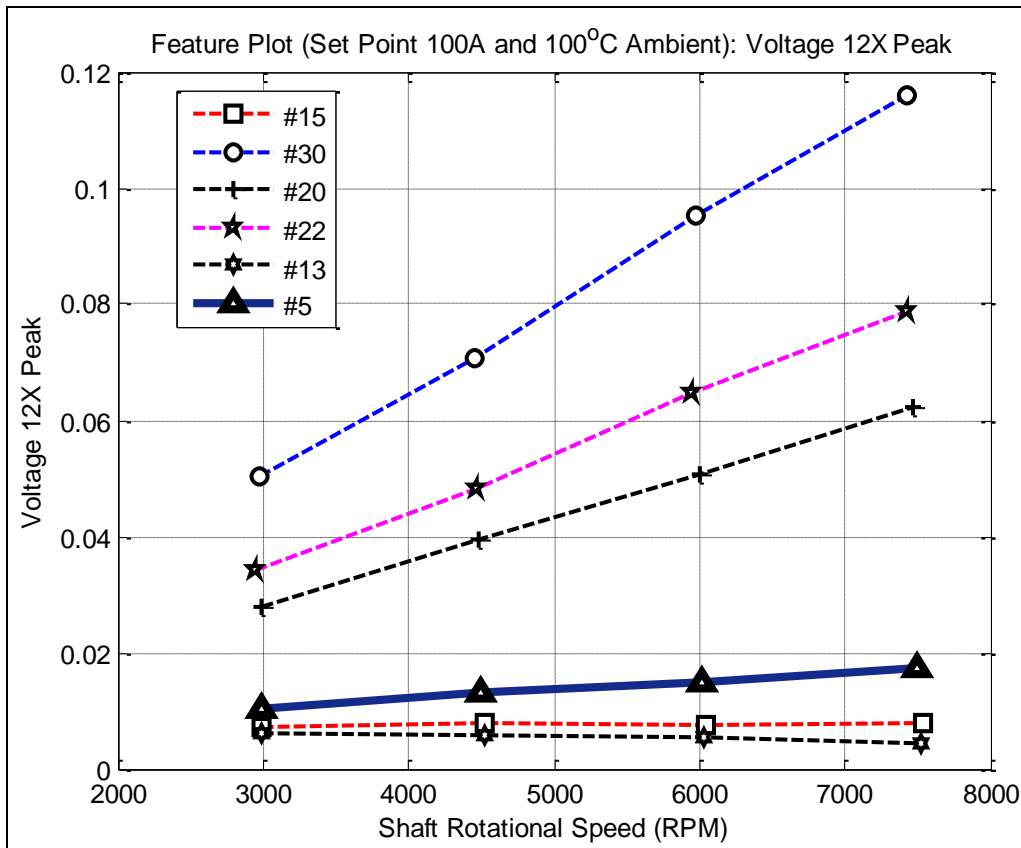
Figure 10. 12X voltage peaks for all alternators tested as a function of shaft speed.

Figure 11 shows the standard deviation in the current ripple. Both the new alternators (#5 and #15) show less variation in the ripple compared to the used alternators. In particular used alternator #30 has significantly higher variation. Note that all that is known about the used

alternators is that they had been in operation on vehicles. No knowledge of how "used" they were is known. This could explain the difference between #30 and the other used alternators.
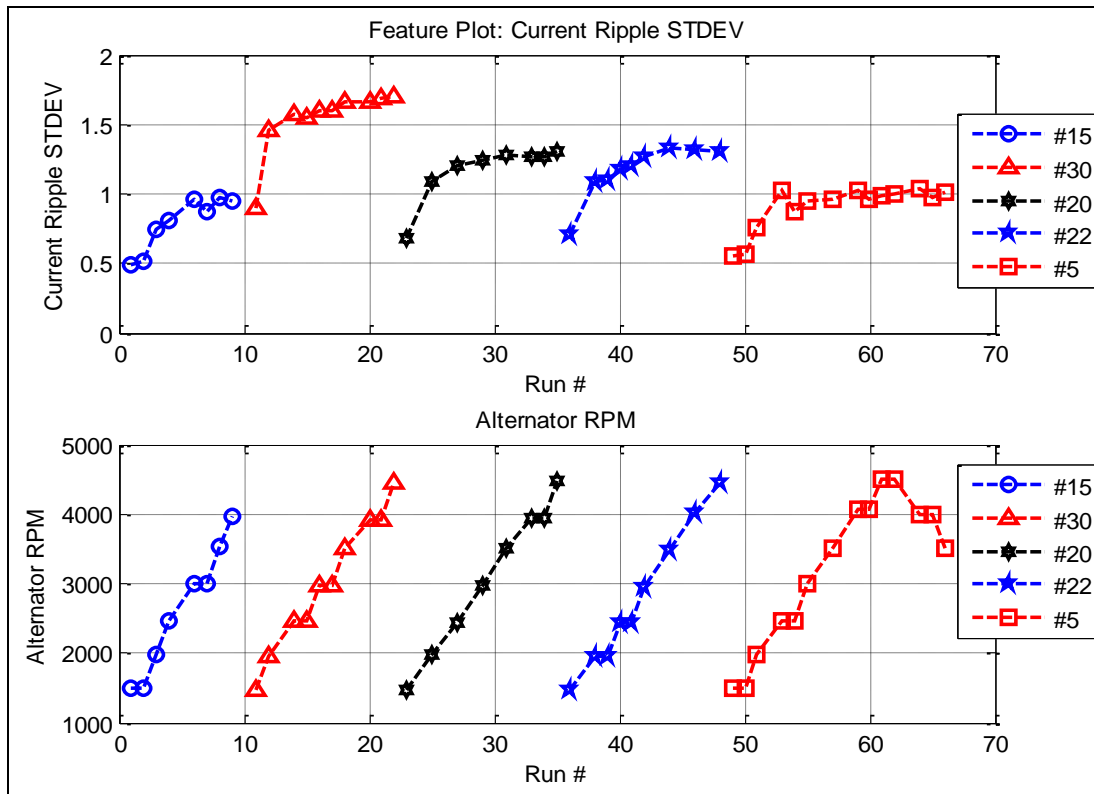
Figure 11. Current ripple standard deviation with the associated shaft speeds for all alternators.

Figure 12 shows the current FOM, FOM_C1, the ratio between the residual current RMS and the TSA current RMS. For the used alternators, the magnitude of this feature is higher and also there appears to be a more noticeable relationship with the increase in shaft speed.
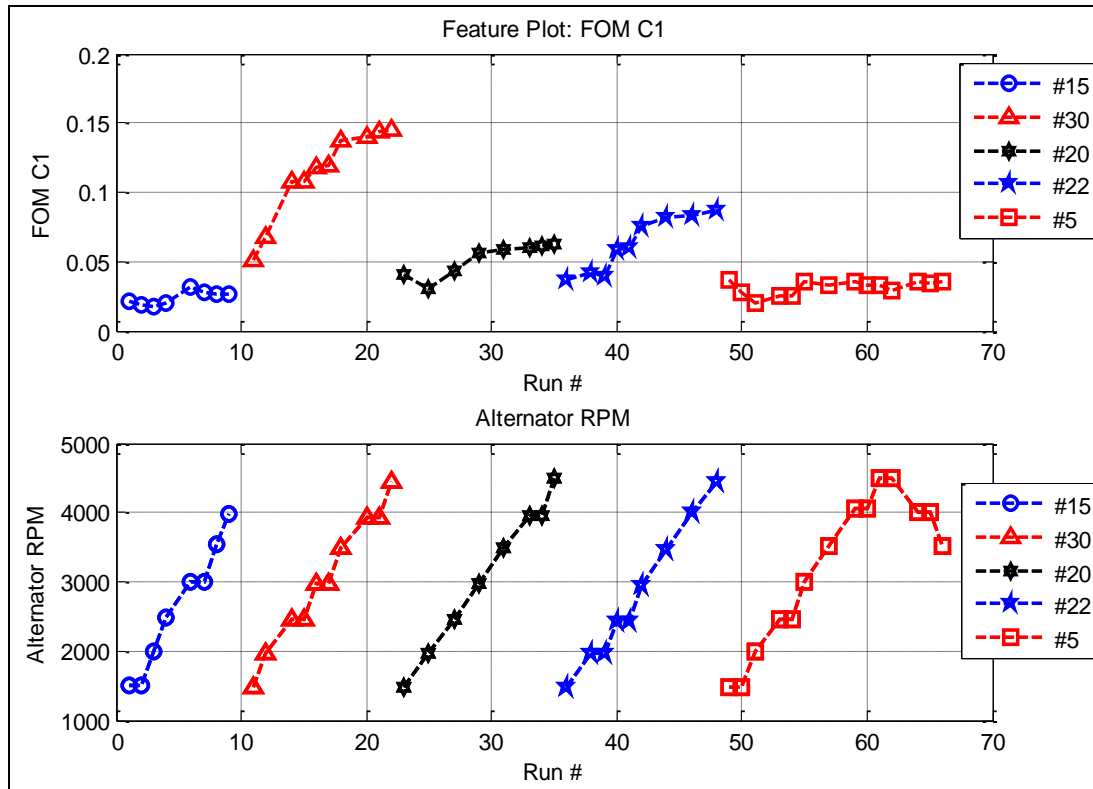
Figure 12. FOM_C1 with the associated shaft speed for all alternators.

Further examination of the results seen in figure 12 was done by looking at the 12X current peak shown in figure 13. Based on the results shown in figure 11, the FOM_C1 behavior is attributed to the 12X current peak. Note that for the used alternators, the 12X current peak is larger in magnitude and exhibits a clearer relationship with shaft speed. Also significant in the current plot is the difference in the frequency dependence of new and used alternators; the new alternators appear to be decreasing with speed as opposed to the used alternators which are clearly increasing, both in a nonlinear fashion.
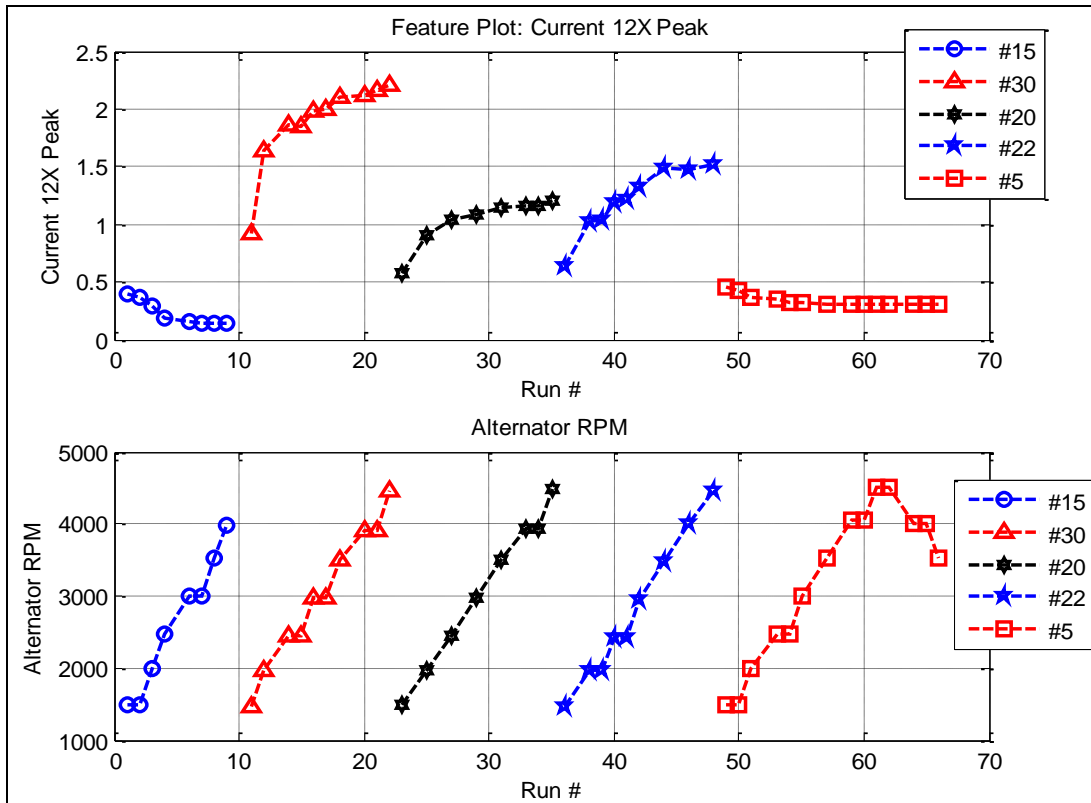
Figure 13. 12X current peaks with the associated shaft speed for all alternators.

The 12X voltage peak shows a similar pattern as the current peaks, as can be seen in figure 14. The peaks are clearly larger for the used alternators. Again, the strong dependence of the 12X peak on speed for the used alternators is noted.

19
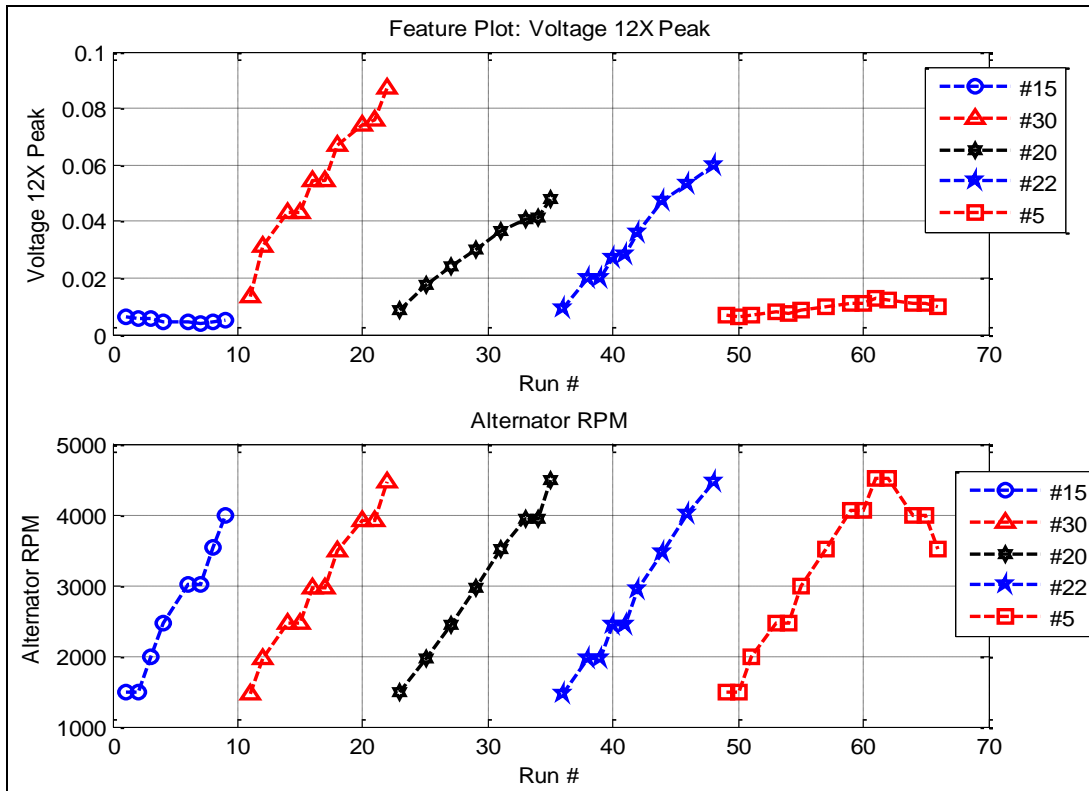
Figure 14. 12X current peaks with the associated shaft speed for all alternators.

The 3X peak from the Y-direction accelerometer is shown in figure 15. It has a noticeable trend for the alternator which failed (#5). However, this is most likely related to shaft misalignment and a function of the test-rig and not the alternator condition.
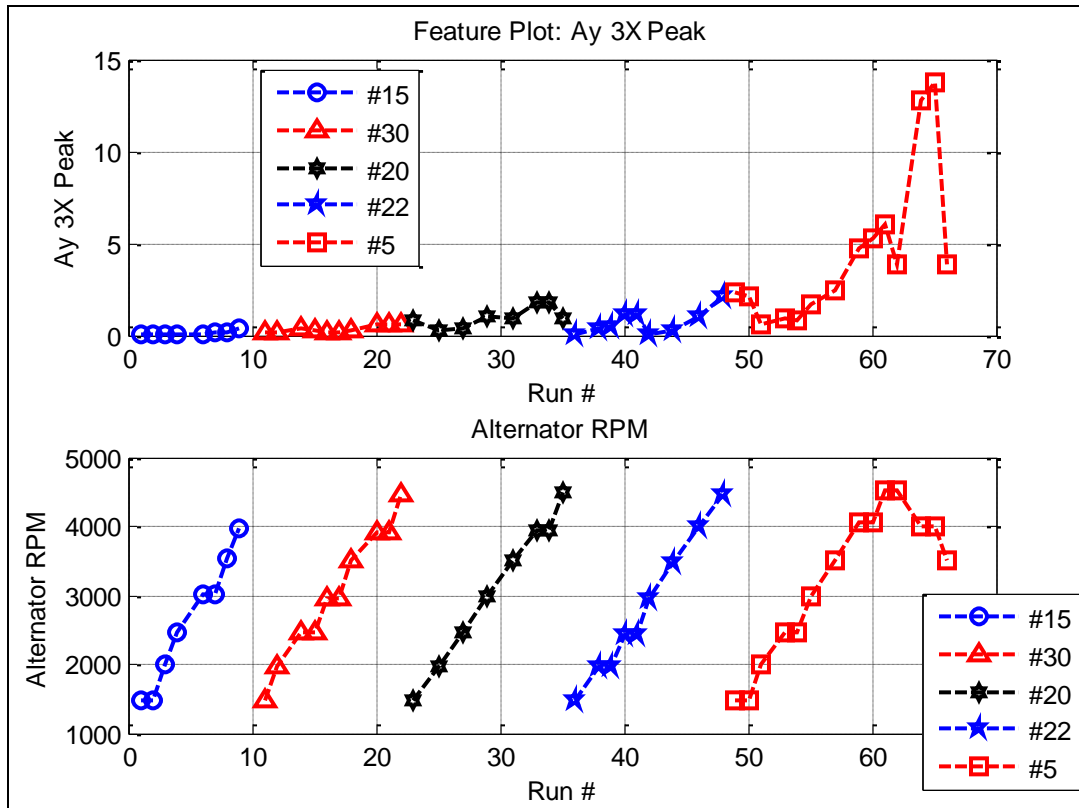
Figure 15. Vibration 3X peak in the Y-direction with the associated shaft speed for all alternators.

Figures 16 and 17 show FOM_3 voltage (FOM_V3) and the kurtosis feature of the regular current signal, respectively. As can be seen, both features are slightly higher for alternator #5 before failure. Whether the levels are significant enough to use as a precursor to failure is uncertain, since it is not possible to test for this given the limited data samples at each operating point.
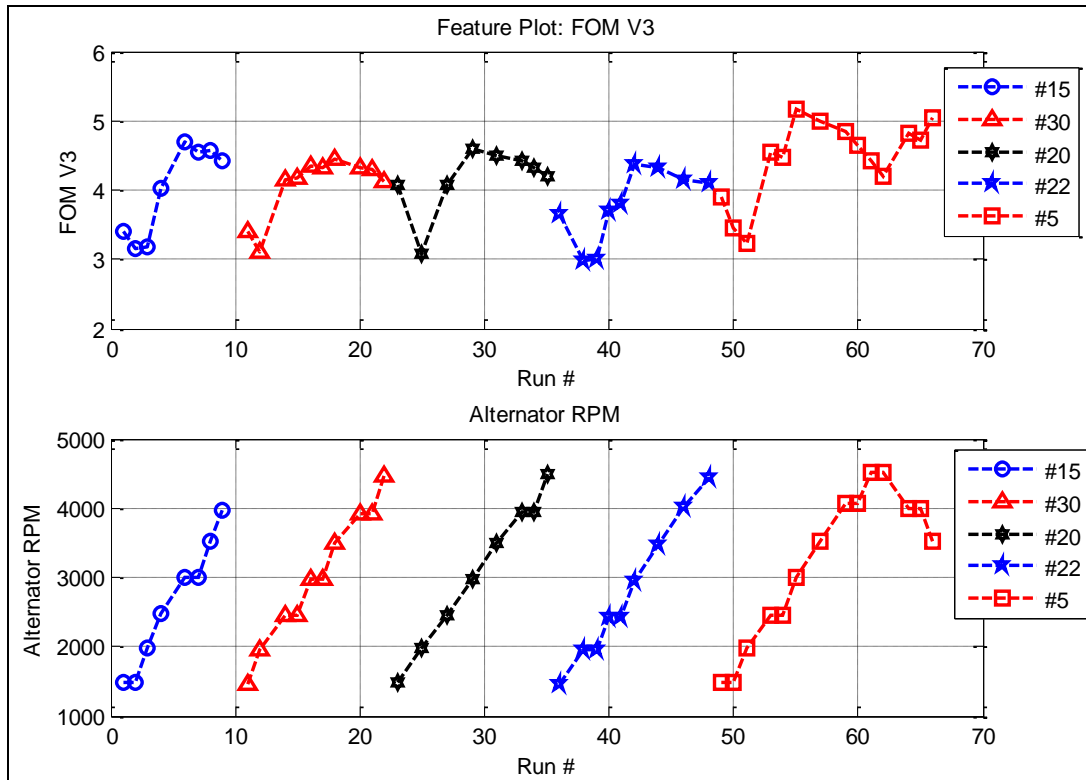
Figure 16. FOM_3-V with the associated shaft speed for all alternators.
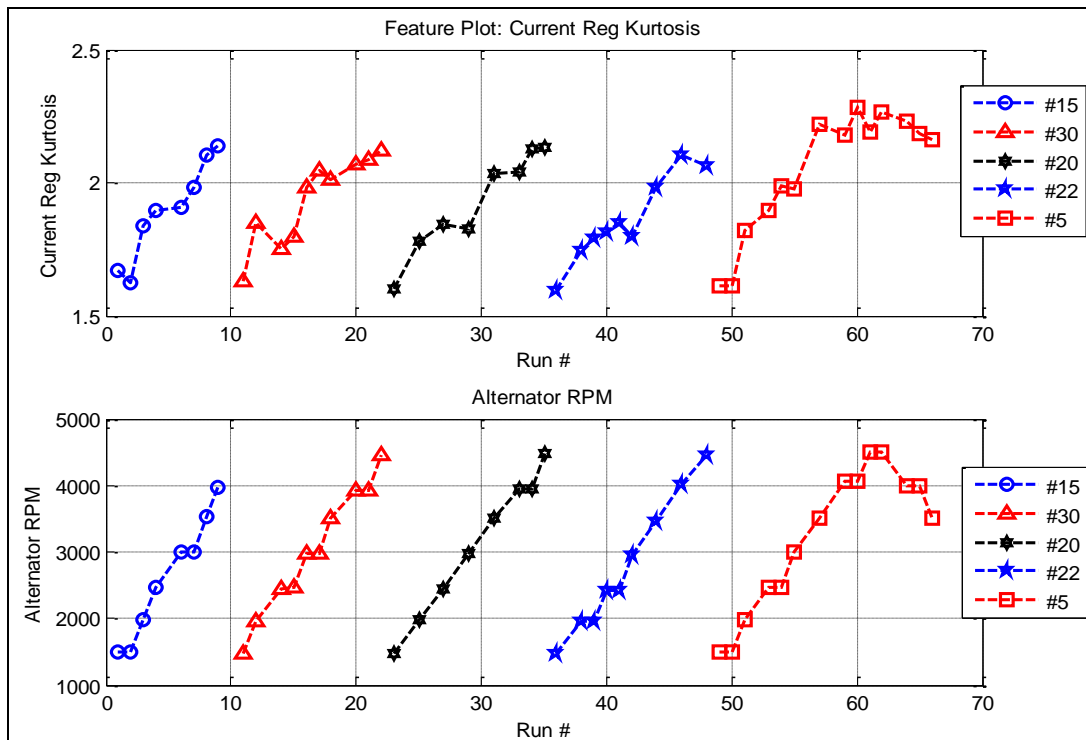
Figure 17. Kurtosis of the regular signal current with the associated shaft speed for all alternators.

5. Discussion

To develop automotive alternator health indicators, the need for additional testing has become apparent. The PSU test procedure was designed for characterization, which appropriately resulted in the data set being constructed of many operating points, unfortunately there were not many replications at a given condition. Several processing methods were applied to the data, and although distinct relationships between rotational speed and several features are observed, none of the methods can confidently provide an early indicator prior to alternator #5 failing. Likewise, although distinct differences in the used and new alternators are apparent, the construction of methodologies to assess state of health or predict remaining useful life is not possible.

6. Conclusions and Recommendations

Observations were made on the PSU alternator data using a wide variety of processing methods and it is believed that these will prove useful in future studies. Several features of interest were identified that have potential for use in the health assessment of automotive alternators given appropriate testing. We first point out that the current/speed output curves for the five alternators represented a normal shape when compared with the manufactures specifications sheet. Also, that the ripple voltage increased with alternator shaft speed, as expected. We note that the used alternators had a distinctly different magnitude for the 12X voltage and current peaks; they also showed a much different relationship with alternator shaft speed. Additionally, the Y-direction vibration 3X peak showed an increasing trend prior to the failure of alternator #5; however, this is likely due to an increasing misalignment or imbalance and not related to the electrical failure. We suggest that to better understand the failure of #5, that the alternator be physically investigated.

Our strongest recommendation is to perform additional testing. Specifically, conducting a set of run-to-failure tests at a fixed operating point (perhaps 80% of rated load at 3000 or 4000 rpm) should provide insight on the signal characteristics/features and how they change over time prior to alternator failure. Also, any additional testing should include collecting the individual phase voltages and currents, since these have a high potential to offer insight on the alternator's condition.

7. References

1. Tactical Wheeled Vehicle Alternator Performance Characterization and Fault Detection Methodology Report, Prepared by The Pennsylvania State University – Applied Research Laboratory, July 1, 2010.

2. Performance Curve for A0014827JB – High Output Alternator Product Specifications, PrestoliteElectric. http://www.prestolite.com/productinfo/alternators/A0014827JB/A0014827JB_curve.jpg (accessed August 2011).

3. Hendrickson, M.; Gottemoller, B. P. Method and Apparatus for Detecting Phase Current Imbalance in a Power Generator, U.S Patent, 20100066294 A1, March 18, 2010.

4. Becker, J.; Jabaji, I.; Patterson, C. System and Method for Generator Phase Signal Monitoring and Control of Electrical Current Distribution, U.S. Patent, 20100138071 A1, June 3, 2010.

5. Zhang, X.; Uliyar, H.; Farfan-Ramos, L.; Zhang, Y.; Salman, M. Fault Diagnosis of Automotive Electrical Power Generation and Storage Systems. *2010 IEEE International Conference on Control Applications*, 2010.

6. Farfan Ramos, L. Real-time Fault Diagnosis of Automotive Electrical Power Generation and Storage System, Master Thesis, Wright State University, Dayton, OH, 2011.

7. Zhang, Y.; Rajagopalan, S.; Salman, M. A Practical Approach for Belt Slip Detection in Automotive Electric Power Generation and Storage System. *IEEE 2010 Big Sky Aerospace Conference*, pp. 1–7, 2010.

8. Banks, J.; Brought, M.; Estep, J.; Hines, J.; Hobbs, N. Health and Usage Monitoring for Military Ground Vehicles Power Generating Devices. *IEEE 2011 Big Sky Aerospace Conference*, pp. 1–17, 2011.

9. Ashemi, A.; Pisu, P. Adaptive Threshold-based Fault Detection and Isolation for Automotive Electrical Systems. *World Congress on Intelligent Control and Automation*, pp. 1013–1018, 2011.

10. Thibedeau, D. G.; Faehnrich, R. J.; Brott, A. P.; Goetzellmann, A. D.; Willems, P. A Alternator Testing Method and System Using Ripple Detection, U.S. Patent, 6,806,727 B2, October 19, 2004.

11. Hamdan, M.; Holler, G.; Grolle, K.; Macnamara, J.; Thakkar, K. System and Method for Detecting Alternator Condition, U.S. Patent, 6,862,504 B2, March 1, 2005.

12. Wang, K. S.; Heyns, P. S. Application of Computer Order Tracking, Vold-Kalman Filtering and EMD in Rotating Machine Vibration. *Mechanical Systems and Signal Processing* **2011**, *25*, 416–430.

13. Decker, H. J.; Zakrajsek, J. J. *Comparison of Interpolation Methods as Applied to Time Synchronous Averaging*; Technical Memorandum, NASA/TM – 1999-209086, ARL-TR-1960; U.S. Army Research Laboratory: Cleveland, OH, 1999.

14. Randall, R. B.; Antoni, J. Rolling Element Bearing Diagnostics – A Tutorial. *Mechanical Systems and Signal Processing* **2011**, *25*, 485–520.

15. Bechhoefer, E.; Kingsley, M. A Review of Time Synchronous Average Algorithms. *Annual Conference of the Prognostics and Health Management Society*, 2009.

16. Guyon, I.; Elisseeff, A. An Introduction to Variable and Feature Selection. *The Journal of Machine Learning Research* **2003**, *3*, 1157–1182.

INTENTIONALLY LEFT BLANK.

Appendix. Data Plots for Reference

Under each heading there are figures for the four alternator "cases" where first figure (top left) is for a new alternator, the figure to its right (top right) is for a used alternator, the third figure (bottom left) is alternator #5 just prior to failure and figure (bottom right) is alternator #5 immediately after failure.

A-1   Current Frequency Spectra (From Raw Signals)
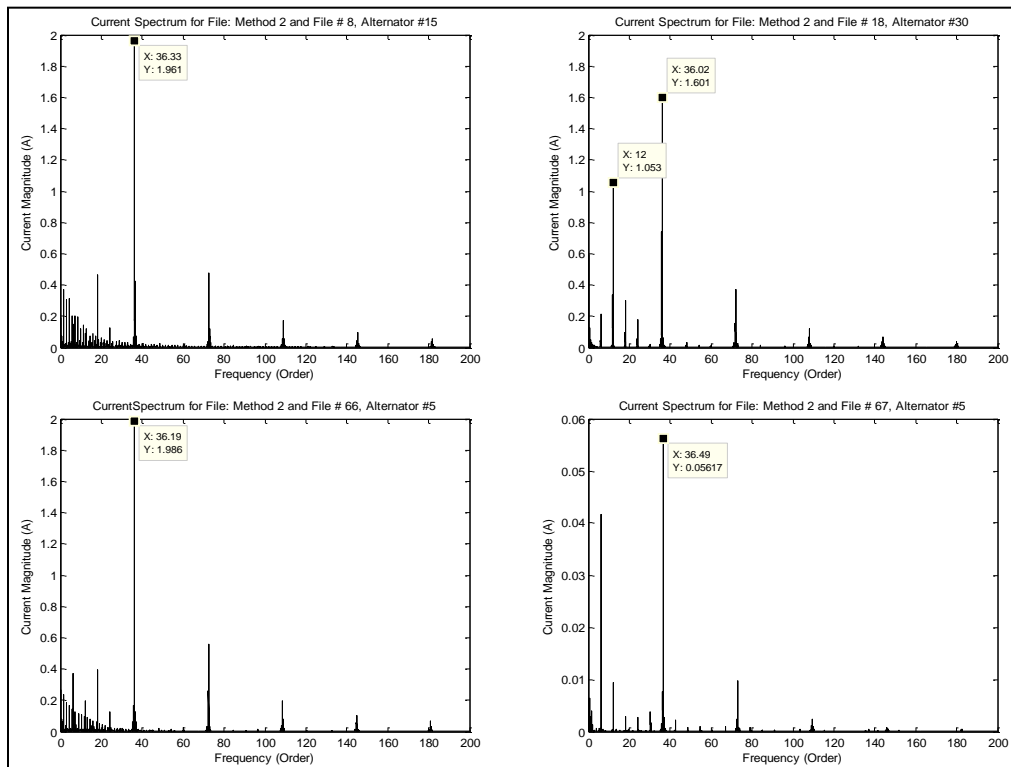
Figure A-1. Frequency spectra for the current output for the four alternator cases.

A-2 Voltage Spectra (From Raw Signals)
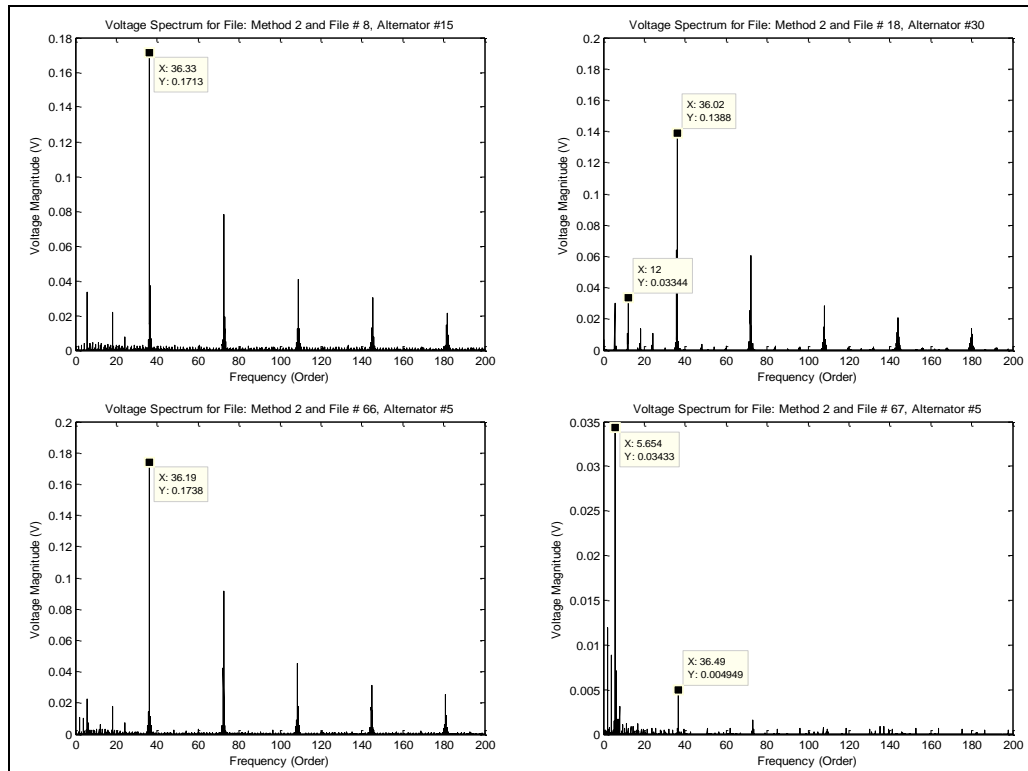
Figure A-2. Frequency spectra for the voltage signal for the four alternator cases.

A-3 Vibration Spectra (From Raw Signals)

A-3.1 X-direction
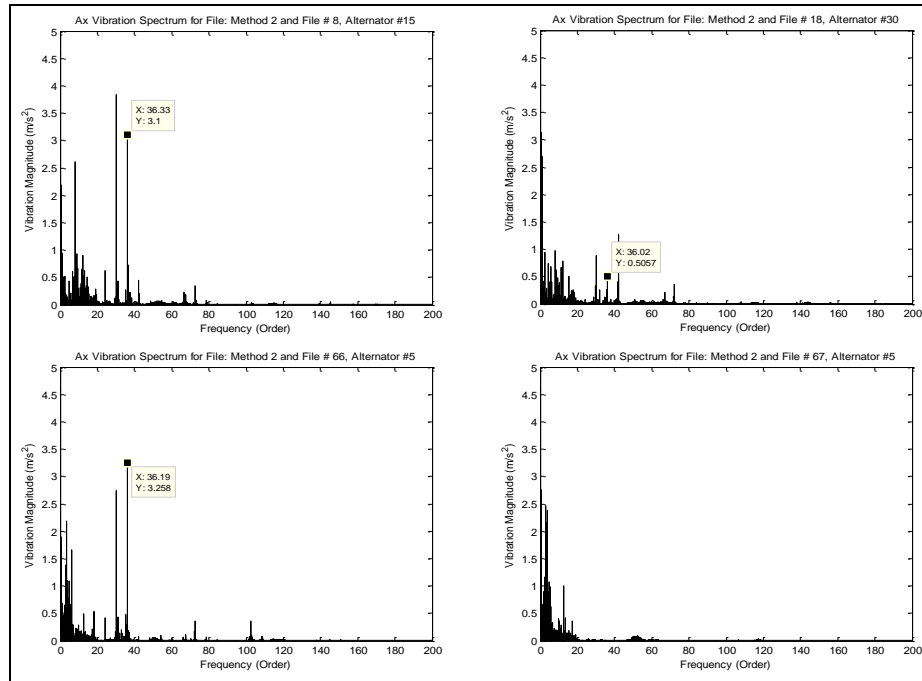
Figure A-3. Vibration spectra for X-direction for the four alternator cases.

A-3.2 Y-direction
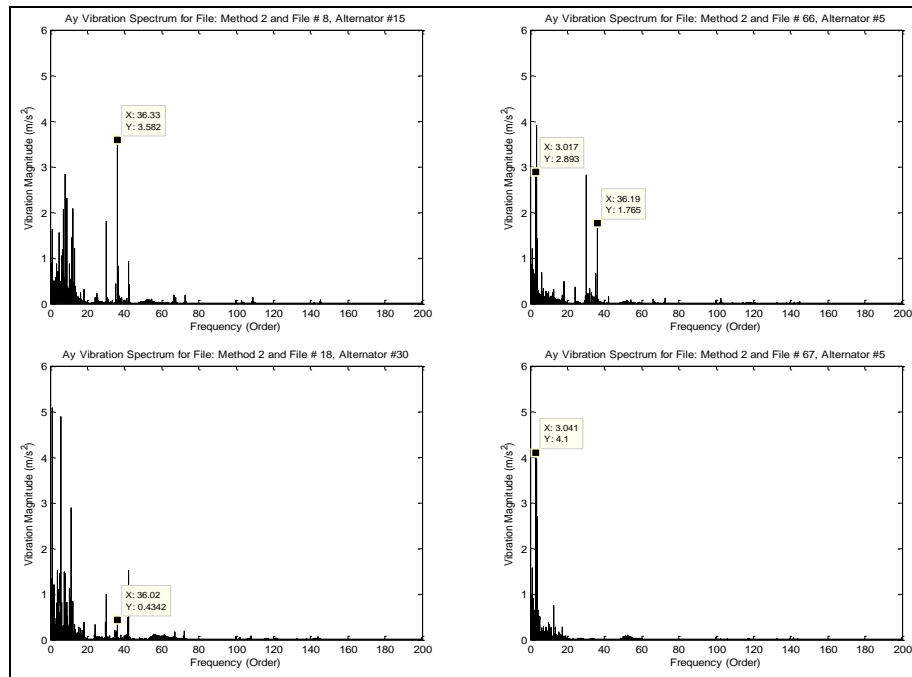
Figure A-4. Vibration spectra for Y-direction for the four alternator cases.

A-3.3 Z-direction
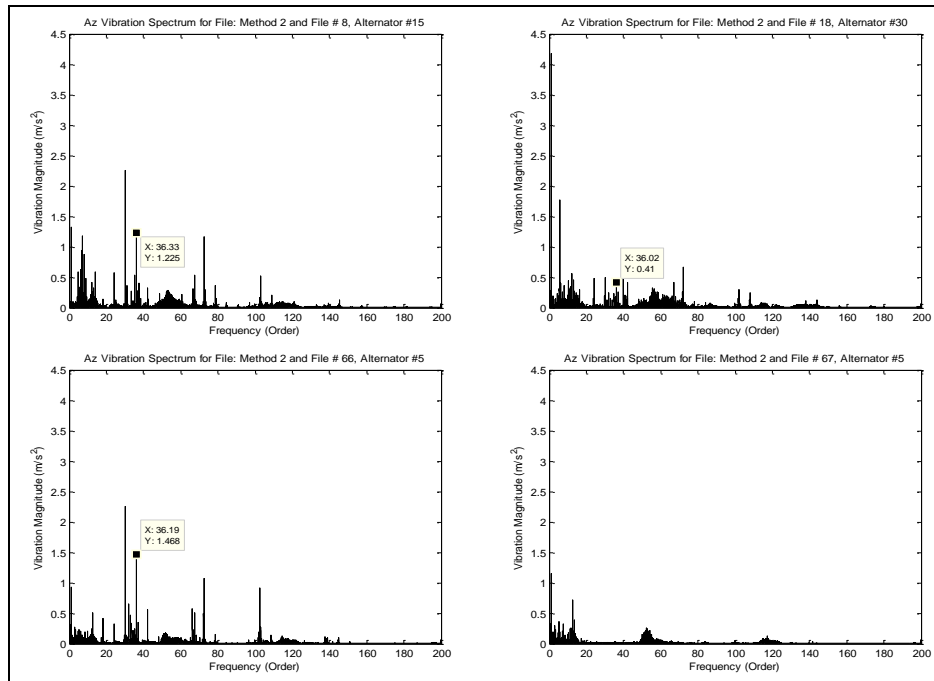
Figure A-5. Vibration spectra for Z-direction for the four alternator cases.

A-4 Time Synchronous Average

A-4.1 Current Spectrum Plots
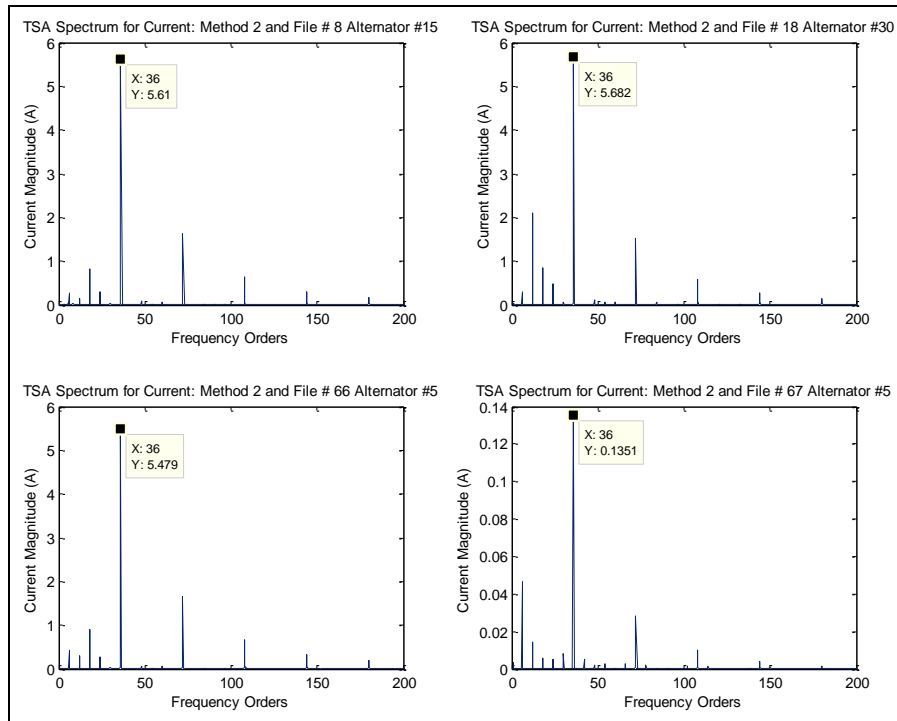
Figure A-6. TSA current spectra for the four alternator cases.

A-4.2 Voltage Spectrum Plots
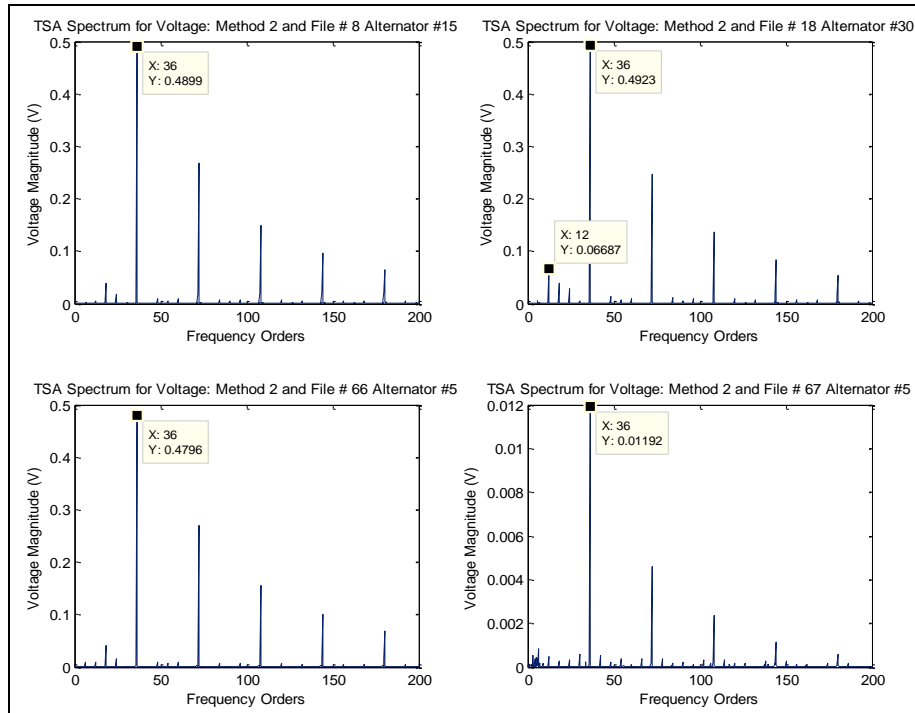
Figure A-7. TSA voltage spectra for the four alternator cases.

A-4.3 Vibration Spectra, X-direction
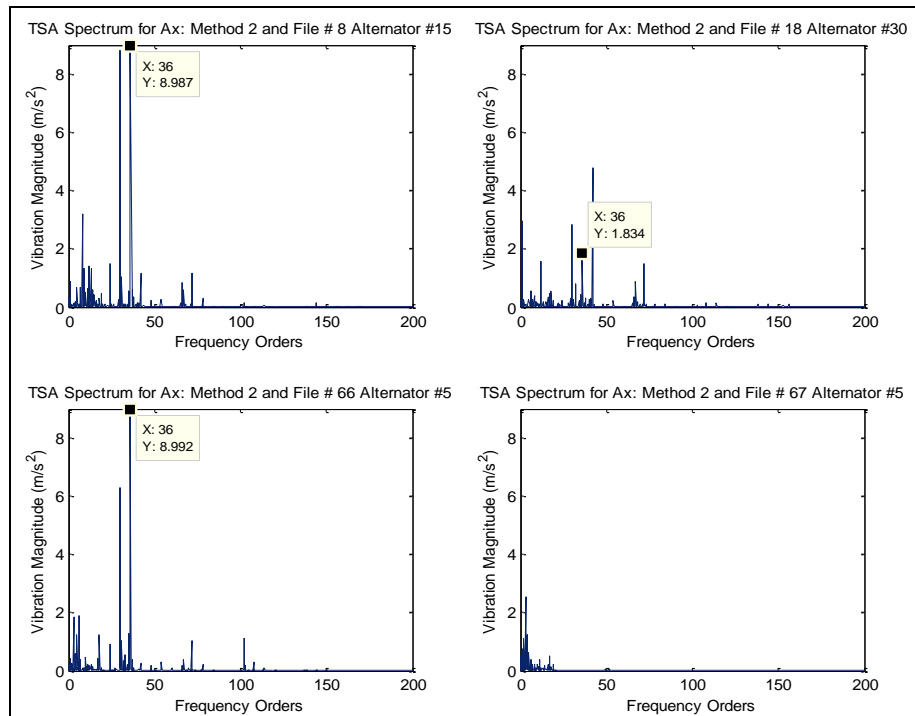
Figure A-8. TSA X-direction vibration spectra for the four alternator cases.

A-4.4 Vibration Spectra, Y-direction
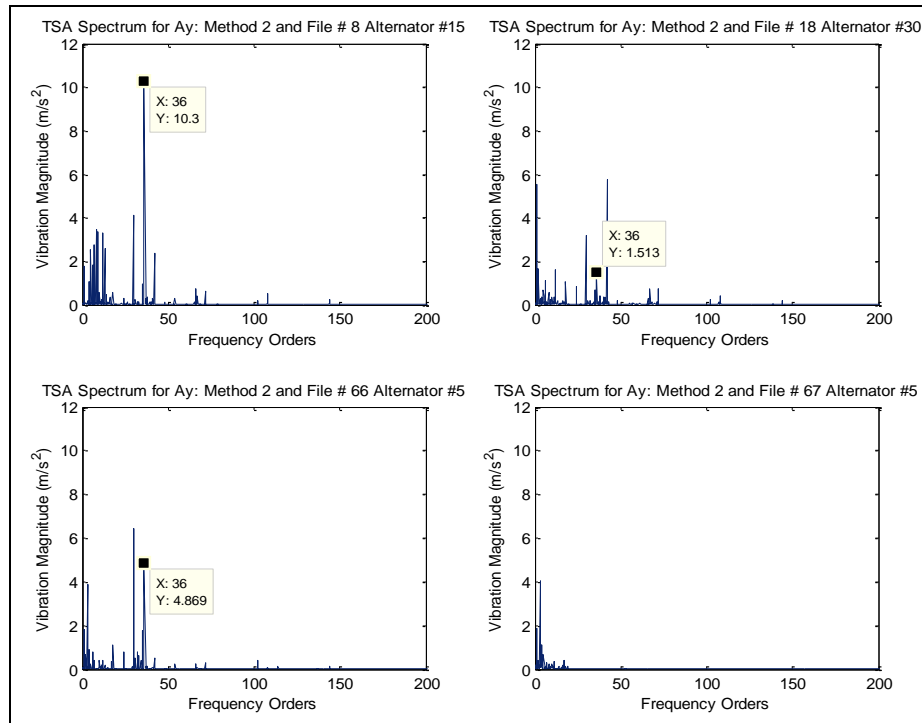
Figure A-9. TSA Y-direction vibration spectra for the four alternator cases.

A-4.5 Vibration Spectra, Z-direction
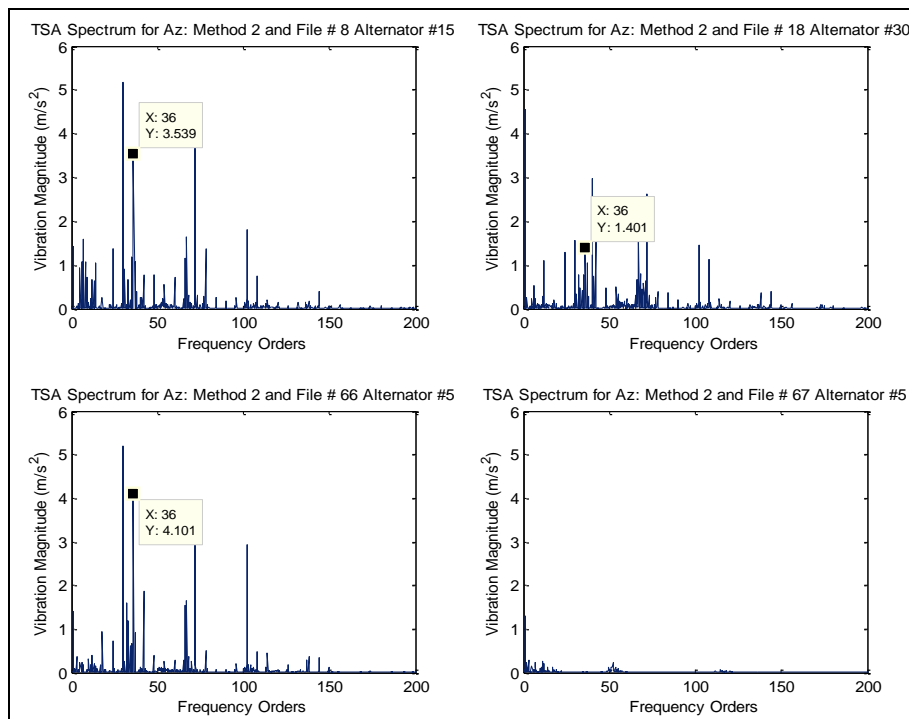
Figure A-10. TSA Z-direction vibration spectra for the four alternator cases.

A-5 Residual Signal

A-5.1 Current
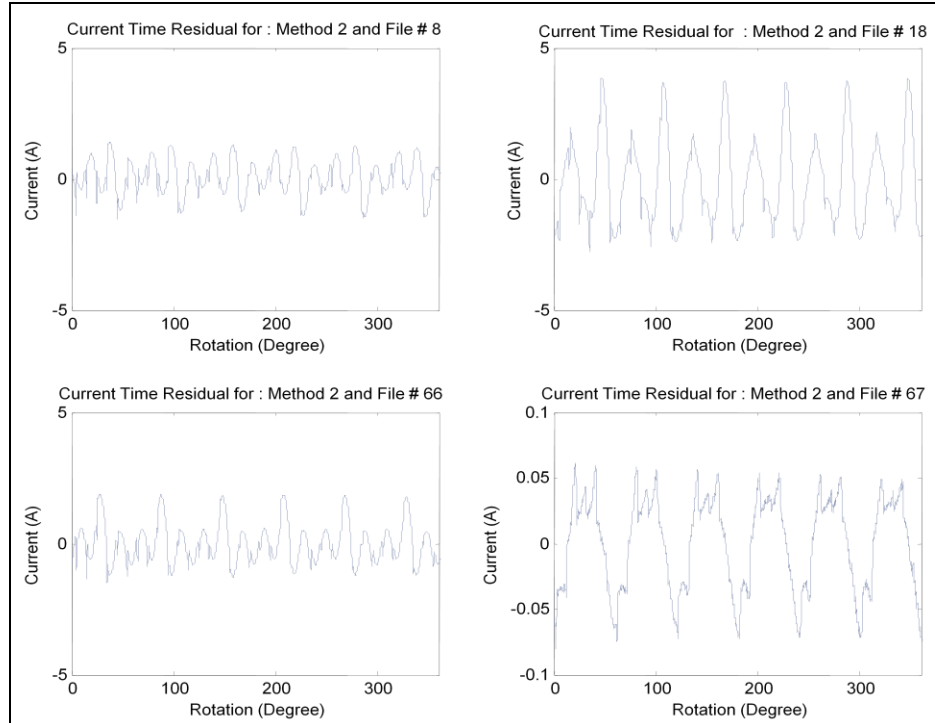
Figure A-11. Current residual for the four alternator cases.

A-5.2 Voltage
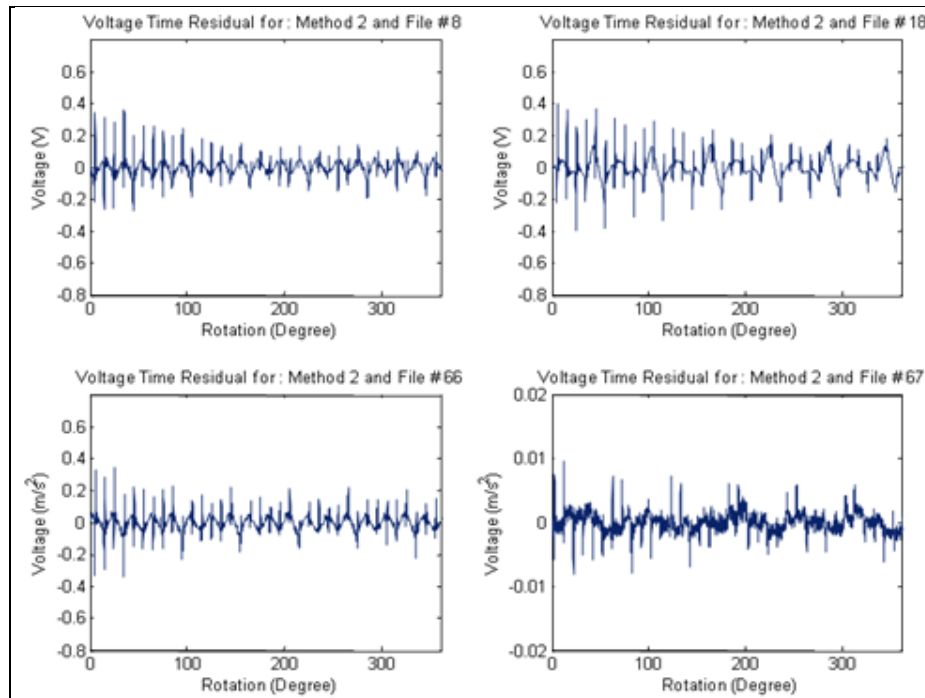
Figure A-12. Voltage residual for the four alternator cases.

A-6 Envelope Signal

A-6.1 Current
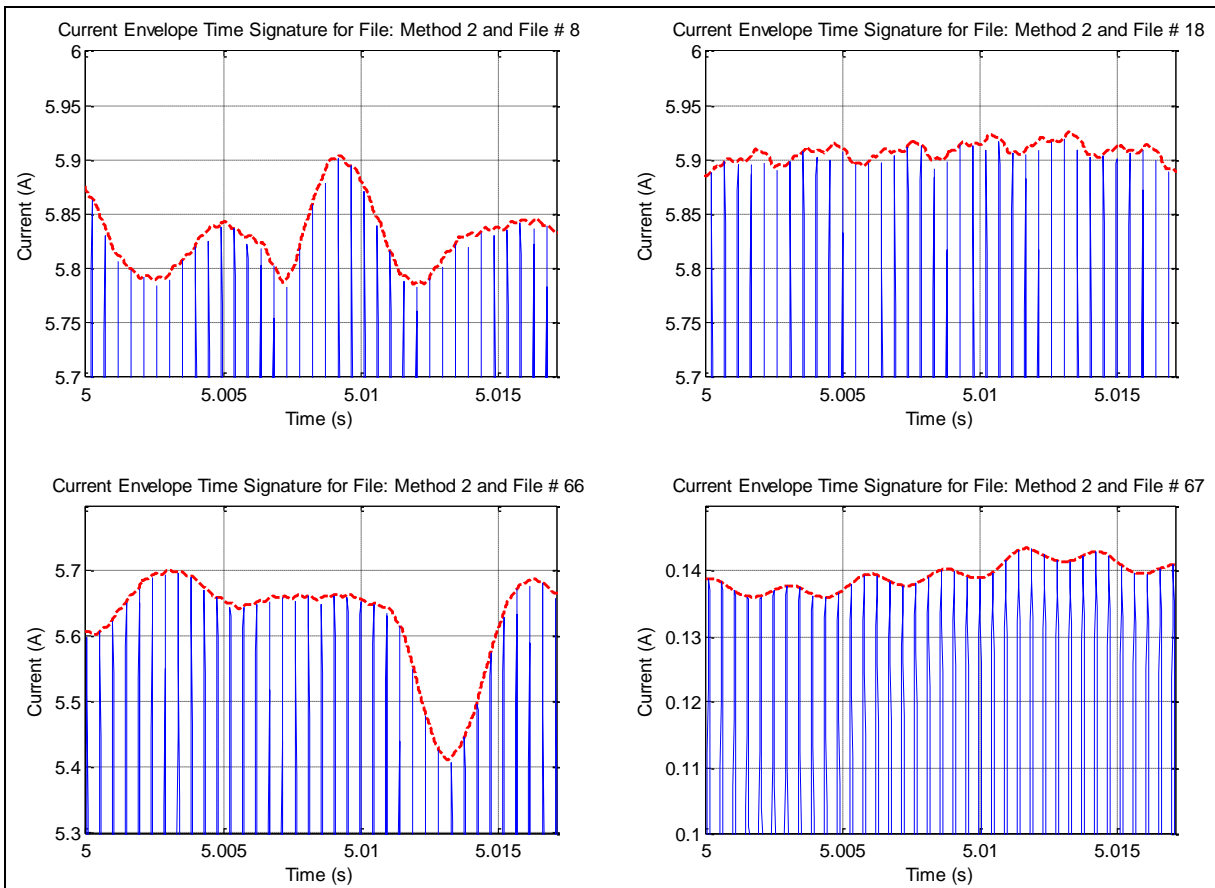
Figure A-13. Current envelope signal for the four alternator cases.

A-6.2 Voltage
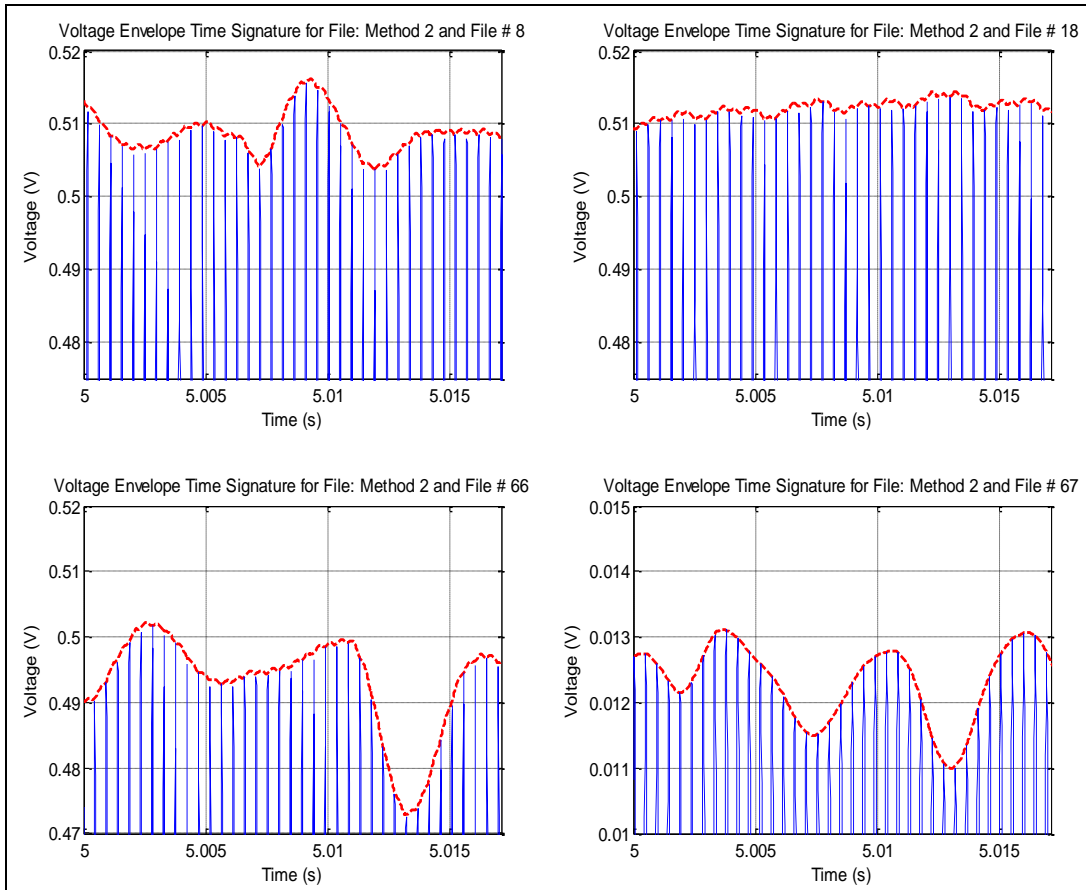
Figure A-14. Voltage envelope signal for the four alternator cases.

A-7 Vibration HFRT Envelope Spectra (X-direction)
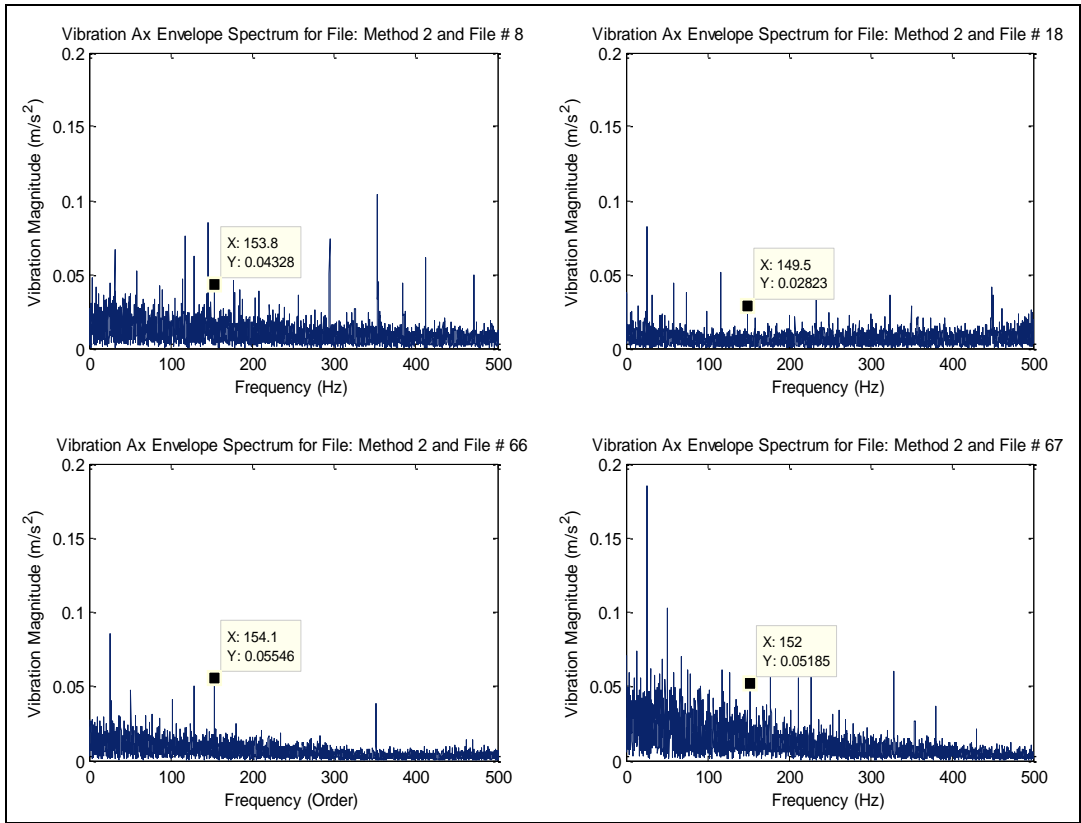
Figure A-15. Vibration envelope spectra (x-direction) showing BPFO.

List of Symbols, Abbreviations, and Acronyms

DoD   Department of Defense

FOMs   figures of merit

HFRT   High Frequency Response Technique

P&D   prognostics and diagnostics

PSU   Pennsylvania State University

RMS   root-mean-square

TARDEC   U.S. Army Tank and Automotive Research, Development and Engineering
            Command

TSA   time synchronous averaging

38